2022 3rd International Conference on Intelligent Engineering and Management (ICIEM) | 978-1-6654-6756-8/22/$31.00 ©2022 IEEE | DOI: 10.1109/ICIEM54221.2022.9853173

Comparing Feature Sets of Pseudo Zernike Moment and Minkowski Functionals to Classify Normal Subjects from COVID Subjects

Dushyanth Balasai J.
Department of Electronics and Communication Engineering
Saveetha School of Engineering
Saveetha Institute of Medical and Technical Sciences
Chennai, India
jakkamdushyanthbalasai17@saveetha.com

Ramesh Munirathinam
Department of Electronics and Communication Engineering
Saveetha School of Engineering
Saveetha Institute of Medical and Technical Sciences
Chennai, India
rameshm.sse@saveetha.com

***Abstract*— Aim: Objective of this study is to analyze the efficiency of Pseudo Zernike Moment in differentiating COVID subjects from controls compared to Minkowski Functionals. Materials and Methods: The data for this study is obtained from a publicly available dataset. By fixing predefined values to the parameters such as effect size and algorithm power as 0.3 and 0.80 in G power tool provides the required sample size as 176. Pseudo Zernike moments and Minkowski features are extracted from the binary lung CT scans. Result: Pseudo Zernike moment feature (M2) is found to have a mean value of 0.63 for normal subjects and 0.56 for COVID subjects. Minkowski area feature is found to have the ability to differentiate COVID subject compared to its other features. Pseudo Zernike features exhibit better statistical significance ($p<0.05$) in differentiating normal and COVID subjects. Neural network classifier shows better classification ability with 91% classification accuracy in separating COVID subjects from normal controls. Conclusion: Compared to Minkowski features, pseudo-Zernike moments has better classification ability to differentiate normal and COVID subjects.**

Keywords— COVID, CT images, Medical Image Processing, Minkowski functionals, Novel shape descriptor, Pseudo Zernike moments

I. INTRODUCTION

The severe acute respiratory syndrome coronavirus 2 (SARSCoV-2) resulting in coronavirus disease 2019 (COVID-19) pandemic presents diagnostic evaluation challenges [1]. Symptoms of some COVID patients include fever, fatigue, cold, cough, runny nose, sore throat, myalgia, etc. whereas a large number of others are asymptomatic [2]. Global statistics provided the number of confirmed cases as on March 2021 as 109,594,835 including 2,424,060 deaths [3]. Non-invasive imaging modalities including X-ray, Computed Tomography (CT) and ultrasound provide valuable information about the changes in human body. However, due to involvement of high radiation X-ray modality is not widely used for the diagnosis of COVID. CT is widely used to detect the changes in soft tissues due to incidence of COVID [4]. This analysis can be used in early diagnosis and treatment planning of COVID.

Around 1124 and 147 articles dealt with COVID and also analysis based on Minkowski features and pseudo-Zernike features were published in google scholar and science direct online repositories over recent years. The two algorithms proposed by Papakostas [5] extracted Zernike and pseudo-Zernike moments faster with 70% less computation time than the direct feature extraction method. Pseudo Zernike moments used by Hosny [6] was extracted at 75% efficient time compared to direct method and provided better results in classification and diagnosis. Arns considered dust, noise of some complexity as random models for the study of Minkowski functionals [7]. David had developed a method for approximating 2D and 3D Minkowski measures. He approached a new method in implementing Minkowski functionals in Matlab software and obtained the final result which was represented in the form of grey level image [8]. Our Teams have previously published in a variety of topics [9]–[30] , To add to this rich experience we have worked on the current study.

Due to the lack of significant classification methods and there exists no unified method for efficient diagnosis and classification of COVID. The aforementioned problems were identified from the literature. The purpose of the study is to evaluate the lung deformation due to incidence of COVID-19 using pseudo-Zernike moments and Minkowski functionals.

II. MATERIALS AND METHODS

The proposed analysis is carried out in the image processing laboratory at Saveetha School of Engineering. Number of samples required for the study is calculated using G-power software tool [31], [32]. The values such as 0.3, 0.05 and 0.8 are fixed for the parameters such as effect size, allowable error and base power of the algorithm. Also, equal number of samples are calculated by fixing the allocation rate as 1. Based on the parameters given a sum of 176 samples are required for better analysis.

CT scans are obtained from Kaggle [33] an open access public repository. A total of 200 images are finalized considering 10 CT scan images from 20 subjects. The images are categorized into normal and COVID subjects.

Softwares such as SPSS and MATLAB are used for efficient analysis [34], [32] and [35]. The proposed workflow is shown in Fig. 1. Lung regions are extracted using the level set method [36]. Pseudo Zernike and Minkowski features are extracted from binary lung image and neural network classifier is used to classify normal from COVID subjects [37].

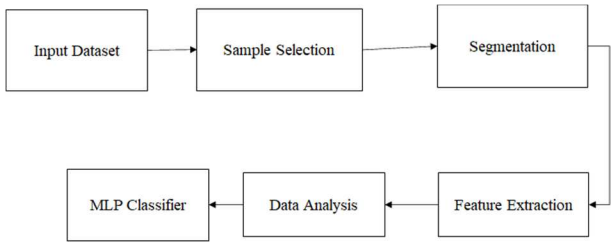

Fig. 1. Workflow of the proposed study to analyze shape alteration of lung using shape features.

A. Pseudo Zernike moments

Pseudo Zernike moments reduce the computation complexity using pseudo Zernike polynomials (Al-Rawi et al. 2010). Pseudo Zernike moments found to be robust to noise compared to traditional Zernike moments hence widely used in image processing applications (Chong et al. 2003). (Tahmasbi et al. 2010).

B. Minkowski Functionals

Minkowski functionals are used as shape measures. They provide robust quantitative measures for orientation. Minkowski measures are structure probe sensitive and high image resolution [38].

C. Statistical Analysis

Extracted feature values are considered to be independent variables. Based on the independent variables the evaluation performance of the classifiers including accuracy and F1 score are derived to estimate the performance of feature values in differentiating COVID subjects from normal controls [34]. Sample t-test is conducted to analyze the statistical significance of feature values between normal and COVID subjects using feature values of p-ZM and Minkowski functionals separately.

III. RESULTS

The typical CT scan images of normal and COVID subjects are represented in Fig. 2 (a-b). Segmented lung binary CT scan images of normal subjects are represented in Fig. 2 (c-d). Fig. 2 (e-f) represent the lung regions of COVID subjects.

Feature values of Minkowski functionals are represented in Table 1. Statistical significance is observed between normal and COVID subjects. Area, area density, euler, euler density, perimeter and perimeter density are considered for the feature extraction. Mean difference between subject groups indicates the shape and texture loss in infected lungs. The mean area of normal and COVID subjects are 614.95, 587.10 respectively. In such a way significant deduction of mean values can be observed in the remaining features of COVID subjects from Table 3.

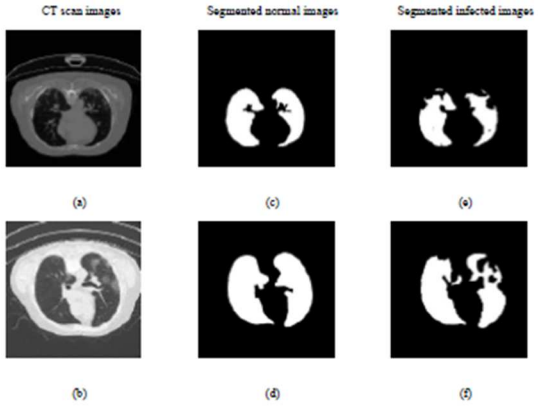

Fig. 2. Representation of (a-b) normal CT scan images, segmented lung regions (c-d) normal subjects, (e-f) COVID subjects

Table 1. Independent sample test is performed using Minkowski features. Area feature obtained, mean difference and standard error difference as 0.508 and 0.02 with p-value 0.01 respectively.

		Levene's Test for Equality of Variances		T-test for Equality of means						
		Mean	Sig	t	dif	Sig (2-tailed)	Mean Difference	Std Error Difference	95% Confidence Interval of the Difference	
									Lower	Upper
Area	Equal variances assumed	1.186	.027	2.423	398	.016	.0508	.020	0.009	.092
	Equal variances not assumed			2.423	396.8	.016	0/20	.021	0.009	.092

Table 2. Independent sample test is performed using pseudo-Zernike moments.

		Levene's Test for Equality of Variances		T-test for Equality of means						
		Mean	Sig	t	dif	Sig (2-tailed)	Mean Difference	Std Error Difference	95% Confidence Interval of the Difference	
									Lower	Upper
M1	Equal variances assumed	21.05	.001	-.996	398	.032	-.0215	.021	-.064	.0209
	Equal variances not assumed			-.996	378.596	.032	-.021	.0216	-.064	.021

The normal and normalised feature values of p-ZM for normal and COVID subjects are shown in Table 4. It is observed that p-ZM feature values are significant between normal and COVID subjects. Particularly second p-ZM (M2) is found to have high significance in classifying COVID

subjects from normal controls. M2 feature values of normal and COVID subjects were (0.63 ± 0.22, 0.56 ± 0.23), these values show differences in normal and infected lungs. In the same way for all 15 features the difference can be observed.

Table 3. Minkowski feature values of normal and COVID subjects. Difference in mean feature values between normal and COVID subjects indicate loss of shape in lungs due to incidence of COVID.

S No	Feature Name	Normal (Mean ± STD)	COVID (Mean ± STD)
1	Area	614.95 ± 109.17	587.10 ± 145.00
2	Area Density	0.001 ± 0.0001	0.001 ± 0.0002
3	Euler 2D	274.48 ± 51.06	269.17 ± 40.45
4	Euler 2D Density	0.001 ± 0.0001	0.001 ± 0.0001
5	Perimeter	898.27 ± 180.85	819.99 ± 120.31
6	Perimeter Density	0.01 ± 0.001	0.009 ± 0.001

STD – Standard Deviation

Graphs have been plotted for extracted features of both Minkowski functionals and pseudo Zernike moments using SPSS software. Fig. 3 represents a statistical analysis graph for extracted pseudo Zernike moment features. On X-axis features were plotted whereas on Y-axis mean values for the features were plotted. Normal feature values have more value than COVID feature values with ±1 standard deviation. Similarly, Fig. 4 represents a statistical analysis graph for extracted Minkowski functional features.

Table 4. Pseudo Zernike moment values of normal and subjects. The moment feature M6 shows a better difference between the normal (1021.13) and COVID (957.57) subjects.

S. No	Feature	Normal		Normalized	
		Normal (Mean ± STD)	COVID (Mean ± STD)	Normal (Mean ± STD)	COVID (Mean ± STD)
1	M1	250.86 ± 56.93	226.09 ± 59.28	0.54 ± 0.19	0.56 ± 0.23
2	M2	438.79 ± 82.91	394.87 ± 91.09	0.63 ± 0.22	0.56 ± 0.23
3	M3	595.40 ± 120.85	548.24 ± 128.39	0.58 ± 0.25	0.53 ± 0.23
4	M4	733.92 ± 124.40	678.40 ± 139.86	0.62 ± 0.23	0.57 ± 0.21
5	M5	880.99 ± 131.55	817.23 ± 144.19	0.61 ± 0.21	0.58 ± 0.20
6	M6	1021.13±13 9.52	957.57 ± 150.73	0.58 ± 0.19	0.63 ± 0.22
7	M7	1155.12 ±149.54	1090.13 ±163.00	0.59 ± 0.19	0.65 ± 0.22
8	M8	1301.40 ±161.85	1237.58 ±175.62	0.60 ± 0.18	0.66 ± 0.22
9	M9	1443.46 ±166.61	1384.56 ±182.73	0.59 ± 0.18	0.65 ± 0.21
10	M10	1596.56 ±167.77	1545.73 ±196.98	0.58 ± 0.18	0.66 ± 0.19
11	M11	1739.11 ±177.62	1696.14 ±216.10	0.56 ± 0.17	0.66 ± 0.19
12	M12	1881.09 ±190.00	1848.30 ±238.22	0.55 ± 0.17	0.64 ± 0.19
13	M13	2032.41 ±200.18	2005.51 ±257.21	0.53 ± 0.17	0.61 ± 0.19
14	M14	2177.40 ±212.26	2157.46 ±276.62	0.52 ± 0.17	0.61 ± 0.20
15	M15	2330.05 ±223.73	2313.59 ±299.33	0.52 ± 0.17	0.60 ± 0.20

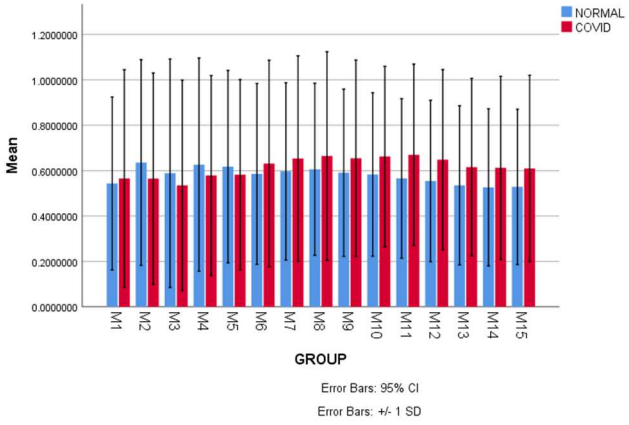

Fig. 3. Symbolic graphs- stat analysis for the extracted pseudo-Zernike moment features. Mean difference with ±1 SD between the normal and COVID subjects of each feature.

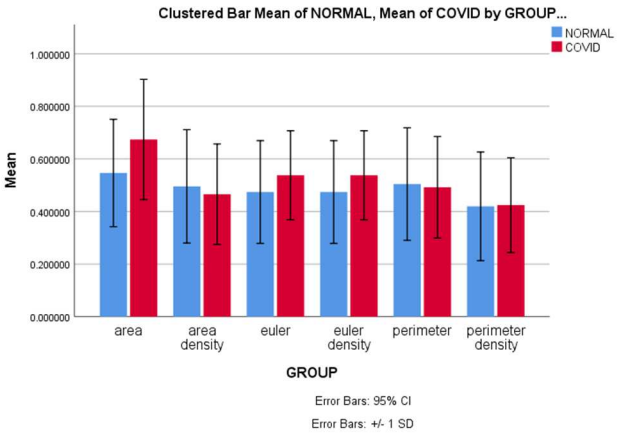

Fig. 4. Representative graphs of the statistical analysis for the extracted Minkowski transform features. Large overlap is observed in the feature values and also there exists high SD between within the features of normal and COVID subjects.

For both normal and normalized feature values of Minkowski functionals and pseudo-Zernike moments the classification ability is performed using a neural network classifier. In Table 5 the classification ability of Minkowski functionals in differentiating normal and COVID subjects is represented.

From Table 5 it is noticeable that normalised feature values perform better than normal feature values in classification purpose. Performance metric values of normalised feature value are 0.897, 0.835, 0.835, 0.837, 0.835 for AUC, CA, F1 score, presion, recall. Similarly in Table 6 classification ability of pseudo Zernike moments in differentiating normal and COVID subjects is represented. Normalized feature values have significant performance metrics with AUC, CA, F1 score, presion, recall of 0.973, 0.912, 0.912, 0.914, 0.912 than the normal feature values. By comparing both the methods through their classification ability, it can be concluded that pseudo Zernike moments have more ability in classifying normal and COVID subjects than Minkowski functionals.

By using classification ability comparison, ROC graphs [39] were plotted for Minkowski functionals and pseudo Zernike moments respectively which is represented in Fig. 5.

Table 5. NN classifier is found to exhibit high performance using normalized features compared to extracted pseudo-Zernike moment features. NN has achieved 91.2% using normalized features which is comparatively higher than the normal features.

Neural Network	AUC	CA	F1 score	Precision	Recall
Normal	0.854	0.765	0.765	0.765	0.765
Normalised	0.973	0.912	0.912	0.914	0.912

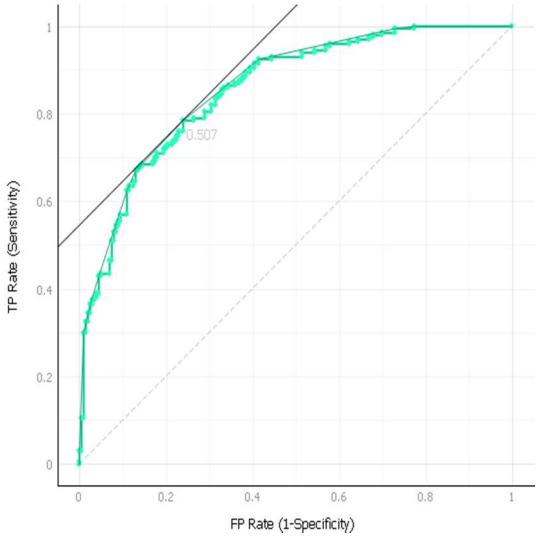

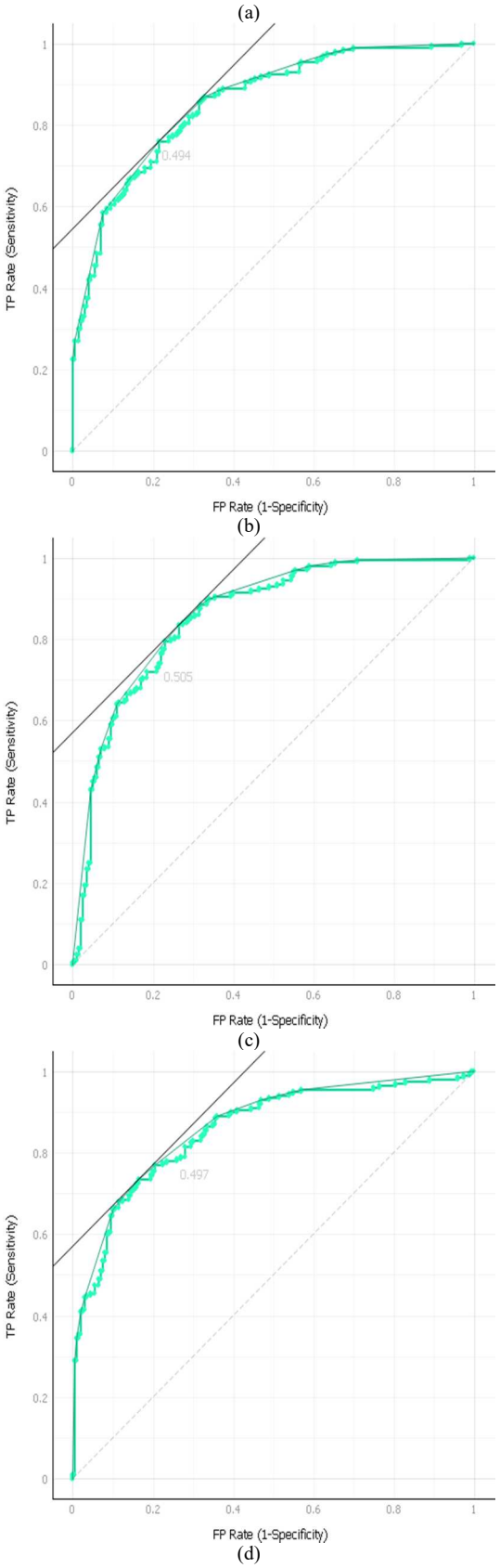

Fig. 5. Representative ROC graphs of (a-b) Minkowski transforms and (c-d) pseudo-Zernike moments. High AUC in pseudo-Zernike moments signify that the false positive rate is greatly reduced

Table 6. Normalized Minkowski features provide improved accuracy (83%) compared to raw features (76%) using NN classifier

Neural Network	AUC	CA	F1 score	Precision	Recall
Normal	0.853	0.762	0.762	0.762	0.762
Normalised	0.897	0.835	0.835	0.838	0.835

IV. DISCUSSION

CT lung images are analyzed to distinguish normal from COVID subjects. It is observed that pseudo-Zernike moments were better than Minkowski functionals to classify COVID subjects from normal subjects using neural network classifiers.

David and his team developed a method for approximating 2D and 3D Minkowski measures. For their study, they used 4 directions in 2D & 13 directions in 3D to obtain efficient accuracy. Proposed a new method of implementing Minkowski functionals in Matlab software. Convergence and non-convergence of an image are measured and the final result was represented as a grey level image. In this study 89% of accuracy is obtained by Minkowski functionals by using the NN classifier. Arns considered dust, blurring and noise of complex random models for the study of Minkowski functionals. He concluded that smoothing affects morphological measures rather than change in particle shape. Here Minkowski functionals were used for measuring the feature values of COVID lung CT images. Timothy used Minkowski functionals in early detection of tumor changes in heterogeneity of MRI images [40]. They used to differentiate T1 weighted images and T2 weighted images before and after the drug treatment [40]. In this study Minkowski functionals were used for early detection of COVID by using CT scan images.
The proposed analysis could be validated using increased number of datasets in near future for effective classification of normal and COVID subjects.

V. CONCLUSION

In this study, Pseudo-Zernike moments and Minkowski features are extracted and analyzed for testing the efficiency of normal and the COVID subjects separately. From the results it is concluded that pseudo Zernike moments has better capability in differentiating normal and COVID subjects with an accuracy of 91% which in higher compared to Minkowski functionals which exhibited the accuracy of 83%.

REFERENCES

[1] O. M. Al-Quteimat and A. M. Amer, "The Impact of the COVID-19 Pandemic on Cancer Patients," American Journal of Clinical Oncology, vol. 43, no. 6. pp. 452–455, 2020. doi: 10.1097/coc.0000000000000712.

[2] X. Ding, J. Xu, J. Zhou, and Q. Long, "Chest CT findings of COVID-19 pneumonia by duration of symptoms," European Journal of Radiology, vol. 127. p. 109009, 2020. doi: 10.1016/j.ejrad.2020.109009.

[3] Ş. Öztürk, U. Özkaya, and M. Barstuğan, "Classification of Coronavirus (COVID -19) from X-ray and CT images using shrunken features," International Journal of Imaging Systems and Technology, vol. 31, no. 1. pp. 5–15, 2021. doi: 10.1002/ima.22469.

[4] Y. Wang et al., "Temporal Changes of CT Findings in 90 Patients with COVID-19 Pneumonia: A Longitudinal Study," Radiology, vol. 296, no. 2, pp. E55–E64, Aug. 2020.

[5] G. A. Papakostas, Y. S. Boutalis, D. A. Karras, and B. G. Mertzios, "Efficient computation of Zernike and Pseudo-Zernike moments for pattern classification applications," Pattern Recognition and Image Analysis, vol. 20, no. 1. pp. 56–64, 2010. doi: 10.1134/s1054661810010050.

[6] K. M. Hosny, "Exact and fast computation of geometric moments for gray level images," Applied Mathematics and Computation, vol. 189, no. 2. pp. 1214–1222, 2007. doi: 10.1016/j.amc.2006.12.025.

[7] C. H. Arns, M. A. Knackstedt, and K. Mecke, "3D structural analysis: sensitivity of Minkowski functionals," J. Microsc., vol. 240, no. 3, pp. 181–196, Dec. 2010.

[8] D. Legland, K. Kiêu, and M.-F. Devaux, "COMPUTATION OF MINKOWSKI MEASURES ON 2D AND 3D BINARY IMAGES," Image Analysis & Stereology, vol. 26, no. 2. p. 83, 2011. doi: 10.5566/ias.v26.p83-92.

[9] S. Gheena and D. Ezhilarasan, "Syringic acid triggers reactive oxygen species-mediated cytotoxicity in HepG2 cells," Hum. Exp. Toxicol., vol. 38, no. 6, pp. 694–702, Jun. 2019.

[10] Y. Ke et al., "Photosynthesized gold nanoparticles from Catharanthus roseus induces caspase-mediated apoptosis in cervical cancer cells (HeLa)," Artif. Cells Nanomed. Biotechnol., vol. 47, no. 1, pp. 1938–1946, Dec. 2019.

[11] M. Vairavel, E. Devaraj, and R. Shanmugam, "An eco-friendly synthesis of Enterococcus sp.-mediated gold nanoparticle induces cytotoxicity in human colorectal cancer cells," Environ. Sci. Pollut. Res. Int., vol. 27, no. 8, pp. 8166–8175, Mar. 2020.

[12] A. Paramasivam, J. Vijayashree Priyadharsini, and S. Raghunandhakumar, "N6-adenosine methylation (m6A): a promising new molecular target in hypertension and cardiovascular diseases," Hypertens. Res., vol. 43, no. 2, pp. 153–154, Feb. 2020.

[13] R. Vignesh, D. Sharmin, C. V. Rekha, S. Annamalai, and P. N. Baghkomeh, "Management of Complicated Crown-Root Fracture by Extra-Oral Fragment Reattachment and Intentional Reimplantation with 2 Years Review," Contemp. Clin. Dent., vol. 10, no. 2, pp. 397–401, Apr. 2019.

[14] I. Saraswathi, J. Saikarthik, K. Senthil Kumar, K. Madhan Srinivasan, M. Ardhanaari, and R. Gunapriya, "Impact of COVID-19 outbreak on the mental health status of undergraduate medical students in a COVID-19 treating medical college: a prospective longitudinal study," PeerJ, vol. 8, p. e10164, Oct. 2020.

[15] R. Ponnulakshmi, B. Shyamaladevi, P. Vijayalakshmi, and J. Selvaraj, "In silico and in vivo analysis to identify the antidiabetic activity of beta sitosterol in adipose tissue of high fat diet and sucrose induced type-2 diabetic experimental rats," Toxicol. Mech. Methods, vol. 29, no. 4, pp. 276–290, May 2019.

[16] S. Dinesh et al., "Influence of wood dust fillers on the mechanical, thermal, water absorption and biodegradation characteristics of jute fiber epoxy composites," J. Polym. Res., vol. 27, no. 1, Jan. 2020, doi: 10.1007/s10965-019-1975-2.

[17] A. C. Gomathi, S. R. Xavier Rajarathinam, A. Mohammed Sadiq, and S. Rajeshkumar, "Anticancer activity of silver nanoparticles synthesized using aqueous fruit shell extract of Tamarindus indica on MCF-7 human breast cancer cell line," J. Drug Deliv. Sci. Technol., vol. 55, no. 101376, p. 101376, Feb. 2020.

[18] F. Chen, Y. Tang, Y. Sun, V. P. Veeraraghavan, S. K. Mohan, and C. Cui, "6-shogaol, a active constiuents of ginger prevents UVB radiation mediated inflammation and oxidative stress through modulating NrF2

signaling in human epidermal keratinocytes (HaCaT cells)," J. Photochem. Photobiol. B, vol. 197, p. 111518, Aug. 2019.
[19] S. Muthukrishnan, H. Krishnaswamy, S. Thanikodi, D. Sundaresan, and V. Venkatraman, "Support vector machine for modelling and simulation of heat exchangers," Therm. Sci., vol. 24, no. 1 Part B, pp. 499–503, 2020.
[20] J. Jose, Ajitha, and H. Subbaiyan, "Different treatment modalities followed by dental practitioners for Ellis class 2 fracture – A questionnaire-based survey," Open Dent. J., vol. 14, no. 1, pp. 59–65, Feb. 2020.
[21] R. T. Anbu, V. Suresh, R. Gounder, and A. Kannan, "Comparison of the Efficacy of Three Different Bone Regeneration Materials: An Animal Study," Eur. J. Dent., vol. 13, no. 1, pp. 22–28, Feb. 2019.
[22] M. Nair, G. Jeevanandan, Vignesh, and S. Emg, "Comparative evaluation of post-operative pain after pulpectomy with k-files, kedo-s files and mtwo files in deciduous molars -a randomized clinical trial," Braz. Dent. Sci., vol. 21, no. 4, pp. 411–417, Oct. 2018.
[23] K. Avinash, S. Malaippan, and J. N. Dooraiswamy, "Methods of Isolation and Characterization of Stem Cells from Different Regions of Oral Cavity Using Markers: A Systematic Review," Int J Stem Cells, vol. 10, no. 1, pp. 12–20, May 2017.
[24] S. P. S. Dinesh, A. V. Arun, K. K. S. Sundari, C. Samantha, and K. Ambika, "An indigenously designed apparatus for measuring orthodontic force," J. Clin. Diagn. Res., vol. 7, no. 11, pp. 2623–2626, Nov. 2013.
[25] H. Venu, V. D. Raju, and L. Subramani, "Combined effect of influence of nano additives, combustion chamber geometry and injection timing in a DI diesel engine fuelled with ternary (diesel-biodiesel-ethanol) blends," Energy, vol. 174, pp. 386–406, May 2019.
[26] S. S. Varghese, H. Thomas, N. D. Jayakumar, M. Sankari, and R. Lakshmanan, "Estimation of salivary tumor necrosis factor-alpha in chronic and aggressive periodontitis patients," Contemp. Clin. Dent., vol. 6, no. Suppl 1, pp. S152–6, Sep. 2015.
[27] S. K. Kamisetty, J. K. Verma, Arun, S. Sundari, S. Chandrasekhar, and A. Kumar, "SBS vs Inhouse Recycling Methods-An Invitro Evaluation," J. Clin. Diagn. Res., vol. 9, no. 9, pp. ZC04–8, Sep. 2015.
[28] A. Muthukrishnan and S. Warnakulasuriya, "Oral health consequences of smokeless tobacco use," Indian J. Med. Res., vol. 148, no. 1, pp. 35–40, Jul. 2018.
[29] L. Govindaraju, P. Neelakantan, and J. L. Gutmann, "Effect of root canal irrigating solutions on the compressive strength of tricalcium silicate cements," Clin. Oral Investig., vol. 21, no. 2, pp. 567–571, Mar. 2017.
[30] S. Panda, N. D. Jayakumar, M. Sankari, S. S. Varghese, and D. S. Kumar, "Platelet rich fibrin and xenograft in treatment of intrabony defect," Contemp. Clin. Dent., vol. 5, no. 4, pp. 550–554, Oct. 2014.
[31] E. Erdfelder, F. Faul, and A. Buchner, "GPOWER: A general power analysis program," Behavior Research Methods, Instruments, & Computers, vol. 28, no. 1. pp. 1–11, 1996. doi: 10.3758/bf03203630.
[32] F. Faul, E. Erdfelder, A. Buchner, and A.-G. Lang, "Statistical power analyses using G*Power 3.1: tests for correlation and regression analyses," Behav. Res. Methods, vol. 41, no. 4, pp. 1149–1160, Nov. 2009.
[33] M. Oda, Y. Hayashi, Y. Otake, M. Hashimoto, T. Akashi, and K. Mori, "Lung infection and normal region segmentation from CT volumes of COVID-19 cases," Medical Imaging 2021: Computer-Aided Diagnosis. 2021. doi: 10.1117/12.2582066.
[34] R. D. Yockey, SPSS® Demystified : A Simple Guide and Reference, 3rd Edition. Routledge, 2017.
[35] Hanselman, Mastering MATLAB 7. Pearson Education India, 2005.
[36] J. Fang, "Level Set Method in Medical Imaging Segmentation," Level Set Method in Medical Imaging Segmentation. pp. 315–340, 2019. doi: 10.1201/b22435-11.
[37] N. Cristianini, "Neural Network (Artificial Neural Network, Backpropagation Network, Connectionist Network, Multilayer Perceptron)," Dictionary of Bioinformatics and Computational Biology. 2004. doi: 10.1002/0471650129.dob0483.
[38] J. Schmalzing and K. M. Gorski, "Minkowski functionals used in the morphological analysis of cosmic microwave background anisotropy maps," Monthly Notices of the Royal Astronomical Society, vol. 297, no. 2. pp. 355–365, 1998. doi: 10.1046/j.1365-8711.1998.01467.x.
[39] "Comparing ROC curves," ROC Curves for Continuous Data. pp. 120–135, 2009. doi: 10.1201/9781439800225-8.
[40] T. J. Larkin et al., "Analysis of image heterogeneity using 2D Minkowski functionals detects tumor responses to treatment," Magn. Reson. Med., vol. 71, no. 1, pp. 402–410, Jan. 2014.